MMA Memo 119

The Optimum Elongation of the MMA A Configuration

Scott M. Foster
National Radio Astronomy Observatory
Socorro, NM 87801

July 21, 1994

Abstract

We consider the optimum north-south elongation for the Millimeter Array A configuration and interferometric arrays in general. The optimum elongation depends primarily on the observational requirements of the array, with a very weak dependance on the latitude. Assuming that the Millimeter Array A configuration will be used primarily for long integrations, we find that the optimum north-south axis ratio is 1.1 for the latitudes of both Mauna Kea ($19.8°N$) and South Baldy ($34°N$). Finally, we present two options for locating an array of this size on the proposed Mauna Kea site.

1 Introduction

In order to maintain as close to a circular beam as possible over as wide a range in declinations as possible, the Millimeter Array should be elongated in the north-south direction (Ge 1992). The optimum amount of this elongation, however, depends on a number of factors related to the types of observations the array is expected to make. For example, an instrument designed to make full synthesis images will, for high enough declinations, have a nearly circular beam for any sufficiently long observation, regardless of the elongation of the array. For an instrument designed for snapshots, the elongation will be a much more critical parameter. In this memo, we consider some of these factors as they affect the A configuration of the proposed Millimeter Array. We find that an optimum axis ratio for the A array is 1.1. Finally, we consider the implications of this value for the proposed Mauna Kea site

2 Simulations

Since the optimum elongation for the array will depend on the types of observations that the array will make, we first have to decide what types of observations are expected from the Millimeter Array A configuration. Since it has lower surface brightness sensitivity than the other configurations, the A array will most likely be used primarily for long integrations. The main factor limiting the duration of an observation will be the opacity of the atmosphere at low elevations. In order to determine the optimum axis ratio for the A array, we simulated 230 GHz observations of a point source at declinations ranging from $-60°$ to $90°$ in increments of $10°$ with arrays of axis ratio 1.0 to 1.8 in increments of 0.1. We located the arrays at a latitude of $19.8°$ north, the latitude of Mauna Kea. We created an array with the desired axis ratio by starting with the A configuration given by Ge (1992) and holding the length of the north-south

axis at a constant 3 km while scaling down the length of the east-west axis. A point source was observed over a range of hour angles such that the airmass never exceeded 1.4 times the airmass at transit. Thus, an object at a declination of -60° was observed for 3.58 hours, while an object at a declination of 20° was observed for 6.32 hours. The longest of the simulated observations was 12 hours for a source at a declination of 90°. The choice of 1.4 time the transit airmass is somewhat arbitrary. This value allows for reasonably long integrations without a substantial increase in system temperature due to the atmospheric opacity. The synthesized beam from each simulated observation was fit with a gaussian using the non-linear Gaussian fitting routine in SDE, and the beam full width at half maximum was recorded for both the major axis and the minor axis.

For each array axis ratio, we calculated two beam shape parameters which measured the deviation of the beam from a circular beam. The first was simply a sum over declination, δ, of the ratio of beam major axis, B_{maj}, to the beam minor axis, B_{min}, minus 1.

$$\sum_{\delta=-60^\circ}^{90^\circ} \frac{B_{maj}(\delta)}{B_{min}(\delta)} - 1 \tag{1}$$

The second parameter was identical to the first with the exception that it was weighted by $cos(\delta)$ to reflect the amount of sky visible at each declination.

$$\sum_{\delta=-60^\circ}^{90^\circ} (\frac{B_{maj}(\delta)}{B_{min}(\delta)} - 1)cos(\delta) \tag{2}$$

The minimum value of each of these parameters, as a function of array axis ratio, indicates a possible choice for the optimum array axis ratio.

3 Results

Table 1 summarizes the results of the basic experiment described above. Note that the minimum in both beam shape parameters occurs at an array axis ratio of 1.1. Note also that the minima are shallow. If the site terrain requires a small deviation from the optimum array elongation, the effect on the mean beam elongation will be small. Table 2 shows the beam axis ratio for each declination and array axis ratio in our grid. A few trends are evident in the data. For a given array axis ratio, the beam axis ratio passes through three minima. Two of these minima result from projection of the elliptical array to a circular pattern at the appropriate elevation. The third minimum, at a declination of 90°, is present because a source at 90° declination never encounters our 1.4 airmass limit, allowing the Earth to carry the array through a half rotation such that a nearly circular beam is created. For all array axis ratios, the beam is very elongated at the southernmost declinations. A more elongated array will marginally improve the beam shape at the extreme southern declinations (-50° to -60°). At the same time, however, a larger array axis ratio will result in elongated beams at most other declinations. Tables 3 and 4 give the beam major axis and beam minor axis in arcseconds for the basic model.

We also ran several variations of the basic experiment to investigate the sensitivity of our results to changes in our intial assumption that the A array will be used primarily for long integrations over the region of the sky where the airmass is within 40% of the transit value.

array axis ratio	$\sum_{\delta=-60^\circ}^{90^\circ} \frac{B_{maj}(\delta)}{B_{min}(\delta)} - 1$	$\sum_{\delta=-60^\circ}^{90^\circ} (\frac{B_{maj}(\delta)}{B_{min}(\delta)} - 1) cos(\delta)$
1.0	5.69	3.62
1.1	**5.28**	**3.39**
1.2	5.33	3.51
1.3	5.62	3.81
1.4	6.07	4.23
1.5	6.56	4.69
1.6	7.16	5.24
1.7	7.80	5.80
1.8	8.44	6.38

Table 1: Beam shape parameters as a function of elongation. Bold faced values are the minima.

We also considered the effects of the terrain on which the array is built. We briefly summarize the results here.

A quick look at a contour map of Mauna Kea, such as the ones in figures 1 and 2, will show that, on Mauna Kea, it is not possible to construct the array on level ground. In order to investigate the effects of building the array on a slope, we repeated our calculations for an array on an east facing slope with a 10% grade and an array on a south facing slope with a 10% grade. For both the east facing array and the south facing array, the optimum array axis ratio was still 1.1. However, the south facing array showed substantially improved beam axis ratios for the far southern declinations. This can be seen by comparing the beam axis ratios in tables 2 and 5. Simply considering the shape of the A configuration beam, the ideal site for the array would be on a south facing slope. Unfortunately, in the case of Mauna Kea, we cannot build on the south facing slope of the mountain since the Mauna Kea Ice Age Natural Area Reserve occupies this space.

Another major assumption which we must consider is the length of the observations which the A configuration will have to perform. We have assumed rather long observations in our initial experiment. There are likely to be situations where shorter observations are possible. Shorter observations push the optimum array axis ratio towards higher values. If we make our observations over the region of the sky where the airmass is within 20% of the transit value, the optimum array axis ratio increases to 1.2. For even shorter observations, between hour angles of -1 hour and 1 hour, the optimum axis ratio increases to 1.3. In the limit of a snapshot at transit, the optimum axis ratio is 1.4. As before, these minima are shallow. A small change in the array axis ratio will not cause a large deviation from the optimum performance.

The realities of scheduling observing time for a major astronomical instrument also force us to consider the possibility that one may not always be able to observe a source at transit. Therefore, we also ran a variation of our basic experiment in which we modeled two hour observations of a point source, ending at the point where the airmass was 1.4 times its value at transit. In this case, the optimum array axis ratio was 1.2, which is slightly less than the optimum array axis ratio in the two hour transit simulation described above.

Finally, although it does not directly affect the Mauna Kea site, we considered the effects of latitude on the optimum array axis ratio. We repeated the basic experiment with an array at a latitude of 34° north, as opposed to Mauna Kea's 19.8° north latitude. The 34° north latitude

δ	1.0	**1.1**	1.2	1.3	1.4	1.5	1.6	1.7	1.8
-60	3.44	**3.31**	3.18	3.05	2.93	2.82	2.72	2.62	2.52
-50	2.31	**2.16**	2.03	1.92	1.81	1.72	1.63	1.55	1.48
-40	1.77	**1.63**	1.52	1.42	1.33	1.25	1.18	1.12	1.07
-30	1.45	**1.33**	1.23	1.14	1.07	1.02	1.07	1.13	1.19
-20	1.25	**1.14**	1.05	1.03	1.11	1.18	1.25	1.33	1.40
-10	1.12	**1.02**	1.07	1.15	1.24	1.32	1.41	1.49	1.57
0	1.04	**1.06**	1.15	1.24	1.34	1.43	1.52	1.61	1.70
10	1.02	**1.11**	1.21	1.31	1.40	1.50	1.59	1.69	1.78
20	1.04	**1.14**	1.24	1.33	1.43	1.53	1.62	1.71	1.81
30	1.04	**1.13**	1.23	1.32	1.42	1.51	1.60	1.69	1.78
40	1.02	**1.11**	1.20	1.28	1.37	1.46	1.54	1.63	1.71
50	1.02	**1.06**	1.14	1.21	1.29	1.37	1.44	1.52	1.59
60	1.07	**1.01**	1.06	1.13	1.19	1.25	1.31	1.38	1.44
70	1.10	**1.06**	1.01	1.04	1.08	1.13	1.17	1.22	1.26
80	1.00	**1.01**	1.03	1.05	1.07	1.09	1.11	1.13	1.14
90	1.00	**1.00**	1.00	1.00	1.00	1.00	1.00	1.00	1.00

Table 2: Beam axis ratios for the basic model as a function of declination for various array axis ratios. Values for the optimum array axis ratio are indicated by bold face.

is roughly that of the VLA as well as the proposed Springerville and South Baldy sites. The change in array latitude had little effect on the optimum array axis ratio. To within 0.05, the optimum value is still 1.1, although the data suggests that a small shift in the optimum value may have occurred.

Eventually, we must choose a type of observation for which to optimize the array shape. Returning to the surface brightness sensitivity argument, our intial model seems like a good choice. We do have some flexibility, however, in the fact that the minima of the beam shape parameters is shallow. Thus, while an A configuration with a elongation of 1.1 is optimized for long integrations though transit, it will also be quite good for shorter observations, as well as off-transit observations.

4 Possible Array Layout on Mauna Kea

The results of the previous section suggest that the A configuration of the Millimeter Array should be less elongated than previously thought. In order to keep the 3 km maximum baseline called for in the Millimeter Array proposal (1990), we will need to increase length of the east-west axis of the array. The larger array, in turn, will be more difficult to fit onto Mauna Kea.

Figures 1 and 2 show two possible positions for the A configuration. The contours in both figures indicate height above sea level and are spaced at 20 m intervals, with the heavy contours spaced at 100 m intervals. The lowest of the heavy contours is 3200 m, while the summit is just short of 4200 m. The greyscale is a composite of shadowing images similar to those in Holdaway (1994) for an elevation of 20° and for 16 azimuths ranging from 0° to 337.5°. Any

δ	1.0	**1.1**	1.2	1.3	1.4	1.5	1.6	1.7	1.8
-60	0.228	**0.241**	0.252	0.262	0.271	0.280	0.287	0.293	0.299
-50	0.155	**0.160**	0.164	0.167	0.170	0.172	0.174	0.176	0.177
-40	0.120	**0.122**	0.124	0.125	0.126	0.127	0.127	0.128	0.129
-30	0.100	**0.100**	0.101	0.101	0.102	0.103	0.109	0.115	0.122
-20	0.086	**0.087**	0.087	0.090	0.096	0.103	0.109	0.116	0.122
-10	0.078	**0.078**	0.083	0.090	0.097	0.103	0.110	0.116	0.123
0	0.073	**0.077**	0.083	0.090	0.097	0.104	0.110	0.117	0.123
10	0.070	**0.077**	0.084	0.091	0.098	0.104	0.111	0.118	0.124
20	0.071	**0.078**	0.085	0.091	0.098	0.105	0.111	0.118	0.124
30	0.071	**0.078**	0.085	0.092	0.099	0.105	0.112	0.118	0.125
40	0.072	**0.079**	0.086	0.093	0.099	0.106	0.113	0.119	0.126
50	0.074	**0.080**	0.087	0.094	0.100	0.107	0.114	0.120	0.127
60	0.079	**0.082**	0.088	0.095	0.102	0.109	0.115	0.122	0.128
70	0.084	**0.088**	0.091	0.098	0.105	0.111	0.118	0.124	0.131
80	0.084	**0.091**	0.099	0.106	0.113	0.120	0.126	0.133	0.139
90	0.087	**0.095**	0.102	0.109	0.116	0.123	0.130	0.136	0.142

Table 3: Beam major axis in arcseconds as a function of declination for various array axis ratios. Values for the optimum array axis ratio are indicated by bold face.

antenna which falls outside the greyscale will have an unobstructed view of any object at an elevation of 20° or more. The heavy, dashed curve marks the part of the boundary of the Mauna Kea Science Reserve closest to the array. The star shows the location of the existing VLBA antenna. Finally, the possible locations of the A array antenna stations are marked by the squares.

The more southern of the potential array locations (figure 1) lies at the edge of the science reserve boundary. In order to fit the array within this boundary while minimizing shadowing effects, we had to move slightly away from the optimum array axis ratio of 1.1 to a ratio of 1.15. This location does have the advantage of proximity to the VLBA site and its associated infrastructure. This will reduce the lengths of roads and power cables needed by the site. This location also has the advantage of being just to the north of a large area which is hidden from Hilo. This area would be ideal for the control buildings and small configurations (Holdaway, 1994). Table 6 lists the beam major axis, beam minor axis and beam axis ratio for this A configuration.

The more northern of the two potential array sites (figure 2) is located further away from the science reserve boundary and takes advantage of some of the flatter terrain found slightly to the north and west. An array with axis ratio of 1.1 fits easily into this area. The control buildings and small arrays could still be located to the south of the A array as above, or possibly on the flat area near the northwest quadrant of the A array. The principal drawback of this site is the distance from the VLBA site and its associated infrastructure. Table 7 lists the beam major axis, beam minor axis and beam axis ratio for this A configuration.

δ	1.0	**1.1**	1.2	1.3	1.4	1.5	1.6	1.7	1.8
-60	0.066	**0.073**	0.079	0.086	0.092	0.099	0.106	0.112	0.118
-50	0.067	**0.074**	0.081	0.087	0.094	0.100	0.107	0.113	0.120
-40	0.068	**0.075**	0.082	0.088	0.095	0.101	0.108	0.114	0.121
-30	0.069	**0.075**	0.082	0.089	0.095	0.101	0.102	0.102	0.102
-20	0.069	**0.076**	0.083	0.087	0.087	0.087	0.087	0.087	0.087
-10	0.069	**0.076**	0.078	0.078	0.078	0.078	0.078	0.078	0.078
0	0.070	**0.073**	0.073	0.073	0.073	0.073	0.073	0.073	0.073
10	0.069	**0.069**	0.070	0.070	0.070	0.070	0.070	0.070	0.070
20	0.068	**0.068**	0.068	0.069	0.069	0.069	0.069	0.069	0.069
30	0.069	**0.069**	0.069	0.069	0.070	0.070	0.070	0.070	0.070
40	0.070	**0.071**	0.072	0.072	0.073	0.073	0.073	0.073	0.074
50	0.073	**0.075**	0.076	0.077	0.078	0.078	0.079	0.079	0.080
60	0.074	**0.081**	0.083	0.084	0.086	0.087	0.088	0.088	0.089
70	0.076	**0.083**	0.090	0.094	0.096	0.099	0.100	0.102	0.103
80	0.084	**0.090**	0.096	0.101	0.106	0.110	0.114	0.118	0.122
90	0.087	**0.094**	0.102	0.109	0.116	0.123	0.130	0.136	0.142

Table 4: Beam minor axis in arcseconds as a function of declination for various array axis ratios. Values for the optimum array axis ratio are indicated by bold face.

5 Acknowledgements

We would like to thank Mark Holdaway, Peter Napier, and Frazer Owen for their contributions to this work.

6 References

Ge, Jing-Ping, 1992, "Further Simulations of (Possible) MMA Configurations", MMA Memo 80.

1990, "The Millimeter Array", Proposal to NSF

Holdaway, M.A., 1994, "MMA Visibility from Hilo and Topographical Shadowing", MMA Memo 112.

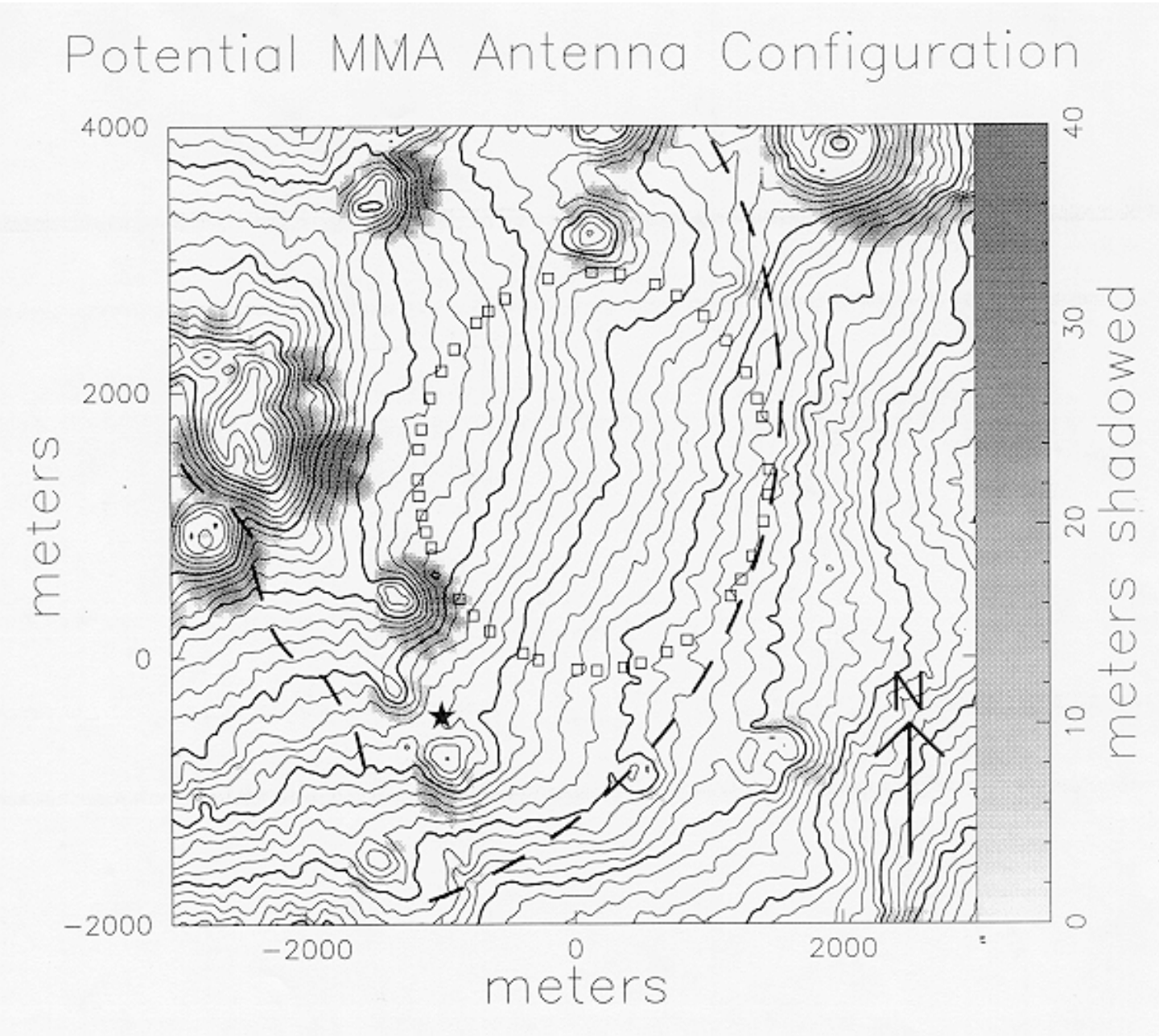

Figure 1: Mauna Kea A array south layout. Contours indicate height above sea level. Dark contours are spaced at 100 m intervals from 3200 m to 4100 m. The greyscale indicates shadowing from an elevation of 20° from all directions. The heavy dashed curve shows part of the Mauna Kea Science Reserve boundary. The star shows the location of the VLBA antenna.

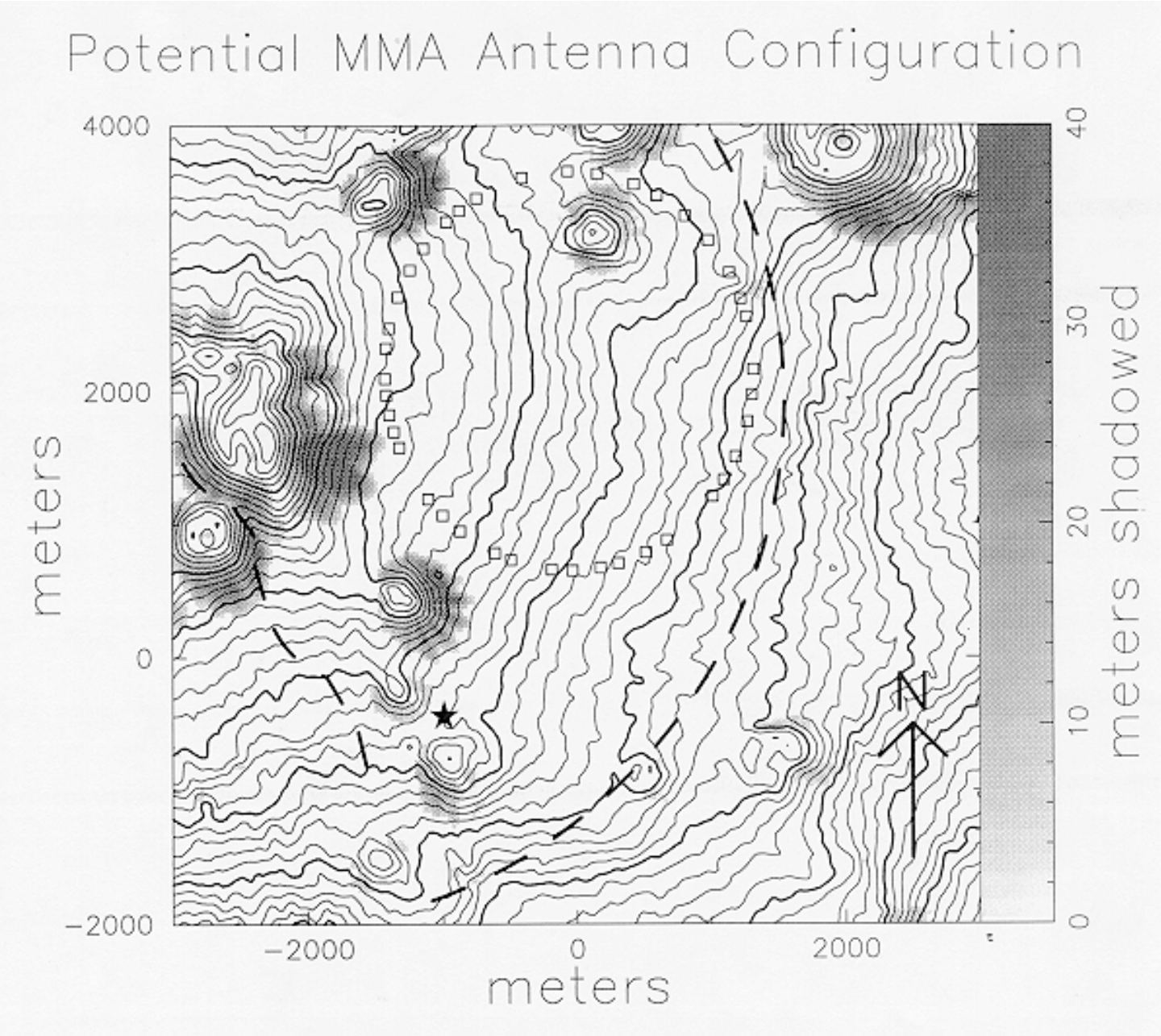

Figure 2: Mauna Kea A array north layout. Contours indicate height above sea level. Dark contours are spaced at 100 m intervals from 3200 m to 4100 m. The greyscale indicates shadowing from an elevation of 20° from all directions. The heavy dashed curve shows part of the Mauna Kea Science Reserve boundary. The star shows the location of the VLBA antenna.

δ	1.0	**1.1**	1.2	1.3	1.4	1.5	1.6	1.7	1.8
-60	2.81	**2.65**	2.50	2.36	2.24	2.13	2.02	1.93	1.84
-50	1.96	**1.82**	1.70	1.59	1.50	1.41	1.33	1.27	1.20
-40	1.55	**1.43**	1.32	1.23	1.15	1.08	1.03	1.05	1.10
-30	1.31	**1.20**	1.11	1.03	1.05	1.12	1.19	1.26	1.33
-20	1.15	**1.05**	1.03	1.12	1.20	1.28	1.37	1.45	1.53
-10	1.06	**1.04**	1.13	1.22	1.32	1.41	1.50	1.59	1.68
0	1.00	**1.10**	1.20	1.30	1.40	1.50	1.59	1.69	1.79
10	1.04	**1.14**	1.24	1.35	1.45	1.55	1.65	1.75	1.85
20	1.05	**1.15**	1.25	1.35	1.45	1.55	1.65	1.75	1.85
30	1.03	**1.13**	1.22	1.32	1.42	1.51	1.61	1.70	1.79
40	1.01	**1.09**	1.18	1.26	1.35	1.44	1.52	1.61	1.70
50	1.05	**1.03**	1.10	1.18	1.25	1.33	1.40	1.48	1.56
60	1.11	**1.05**	1.02	1.08	1.14	1.20	1.26	1.32	1.38
70	1.15	**1.10**	1.06	1.02	1.03	1.07	1.12	1.16	1.20
80	1.02	**1.01**	1.01	1.03	1.04	1.06	1.08	1.10	1.12
90	1.00	**1.00**	1.00	1.00	1.00	1.00	1.00	1.00	1.00

Table 5: Beam axis ratios for an array on a south facing slope as a function of declination for various array axis ratios. Values for the optimum array axis ratio are indicated by bold face.

	Natural Weighting				Uniform Weighting			
δ	$\frac{B_{maj}}{B_{min}}$	B_{maj}	B_{min}	θ	$\frac{B_{maj}}{B_{min}}$	B_{maj}	B_{min}	θ
-60	2.92	0.221	0.076	5.6	2.54	0.157	0.062	3.3
-50	1.95	0.149	0.077	6.3	1.71	0.111	0.065	3.4
-40	1.49	0.116	0.078	8.1	1.38	0.092	0.066	3.4
-30	1.24	0.096	0.078	11.8	1.16	0.080	0.069	0.8
-20	1.09	0.085	0.078	27.0	1.03	0.072	0.070	-10.2
-10	1.07	0.081	0.075	66.6	1.05	0.071	0.068	-72.0
0	1.13	0.080	0.071	81.4	1.12	0.072	0.065	-86.3
10	1.18	0.081	0.069	85.1	1.13	0.072	0.064	-84.0
20	1.19	0.081	0.068	87.5	1.12	0.072	0.064	-88.1
30	1.17	0.082	0.069	89.4	1.10	0.072	0.066	-85.0
40	1.14	0.082	0.072	-88.4	1.09	0.072	0.066	-89.7
50	1.08	0.083	0.077	-83.4	1.05	0.072	0.069	-81.9
60	1.03	0.086	0.083	-54.2	1.02	0.072	0.071	-76.5
70	1.06	0.092	0.087	-13.7	1.01	0.072	0.072	55.2
80	1.01	0.096	0.094	-78.2	1.00	0.072	0.072	-64.4
90	1.00	0.099	0.099	83.8	1.00	0.072	0.072	-52.2

Table 6: Beam axis ratio, beam major axis, beam minor axis and angle between beam major axis and north as a function of declination for both natural and uniform weighting for the Mauna Kea south A array.

δ	Natural Weighting				Uniform Weighting			
	$\frac{B_{maj}}{B_{min}}$	B_{maj}	B_{min}	θ	$\frac{B_{maj}}{B_{min}}$	B_{maj}	B_{min}	θ
-60	3.15	0.228	0.072	5.1	2.76	0.169	0.058	3.1
-50	2.09	0.154	0.073	5.5	1.83	0.113	0.061	1.6
-40	1.60	0.119	0.074	6.7	1.46	0.093	0.063	4.4
-30	1.32	0.098	0.075	8.8	1.22	0.080	0.066	5.8
-20	1.14	0.086	0.075	15.8	1.09	0.073	0.067	5.3
-10	1.05	0.079	0.075	39.0	1.00	0.068	0.068	23.3
0	1.07	0.077	0.072	75.2	1.09	0.070	0.064	86.9
10	1.12	0.077	0.070	83.1	1.08	0.069	0.064	89.8
20	1.14	0.078	0.068	86.7	1.08	0.069	0.064	90.0
30	1.13	0.078	0.069	89.2	1.08	0.070	0.065	89.8
40	1.10	0.079	0.072	-88.0	1.06	0.070	0.066	90.0
50	1.05	0.080	0.076	-80.3	1.06	0.070	0.066	-88.8
60	1.03	0.083	0.080	-32.5	1.01	0.070	0.069	-77.0
70	1.07	0.089	0.083	-10.6	1.00	0.070	0.070	2.1
80	1.01	0.091	0.090	-75.3	1.01	0.070	0.069	-63.7
90	1.00	0.095	0.094	84.3	1.00	0.070	0.070	19.7

Table 7: Beam axis ratio, beam major axis, beam minor axis and angle between beam major axis and north as a function of declination for both natural and uniform weighting for the Mauna Kea north A array.